NANO LETTERS

Letter

pubs.acs.org/NanoLett

Hard X-ray Detection Using a Single 100 nm Diameter Nanowire

Jesper Wallentin,*[,†] Markus Osterhoff,[†] Robin N. Wilke,[†] Karl-Magnus Persson,[§] Lars-Erik Wernersson,[§] Michael Sprung,[‡] and Tim Salditt[†]

[†]Institute for X-ray Physics, University of Göttingen, Friedrich-Hund-Platz 1, 37077 Göttingen, Germany

[‡]DESY, Notkestrasse 85, 22607 Hamburg, Germany

[§]Department of Electrical and Information Technologies, Lund University, Lund S-221 00, Sweden

S *Supporting Information*

ABSTRACT: Submicron sized sensors could allow higher resolution in X-ray imaging and diffraction measurements, which are ubiquitous for materials science and medicine. We present electrical measurements of a single 100 nm diameter InP nanowire transistor exposed to hard X-rays. The X-ray induced conductance is over 5 orders of magnitude larger than expected from reported data for X-ray absorption and carrier lifetimes. Time-resolved measurements show very long characteristic lifetimes on the order of seconds, tentatively attributed to long-lived traps, which give a strong amplification effect. As a proof of concept, we use the nanowire to directly image an X-ray nanofocus with submicron resolution.

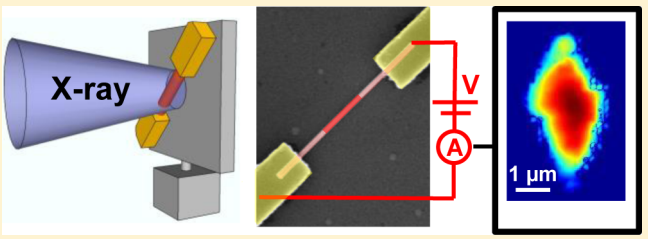

KEYWORDS: *Nanowires, X-rays, detector, III−V*

While hard X-rays can now be focused to sizes around and below 10 nm,[1−4] their direct detection by semiconductor sensors is still based on pixel sizes of tens of micrometers with several hundred micrometer thickness.[5] Direct-detection semiconductor sensors rely on the conversion of X-ray photon energy into an electric signal. First, a hard X-ray photon is absorbed by an electron through photoelectric absorption. The primary high-energy electron releases its energy to the surrounding lattice, creating an avalanche of secondary electron−hole pairs that can be detected electronically.[6,7] However, these nonequilibrium charge carriers quickly recombine, with a characteristic lifetime of about 1−100 ns in direct bandgap semiconductors such as InP.[8,9] The detectable number of electron−hole pairs depends on the competition between generation and recombination.

The primary X-ray absorption scales with the volume, which intuitively leads to a low number of carriers for small pixels. However, for very small semiconductors, i.e., nanostructures, the lifetime of the secondary electron−hole pairs can be substantially different from bulk since the recombination can be affected by surface states and quantum confinement.[10] One type of nanostructure is semiconductor nanowires, which have shown promising performance in fields as diverse as battery anodes,[11] transistors,[12] solar cells,[13] phase-change materials,[14] and quantum physics,[15] as well as detection of light in the infrared to ultraviolet range.[16−18] Because of their long penetration depth, hard X-rays are uniquely suitable for in situ studies of battery anodes[19] and hydrated cells,[20] and have also been used to characterize nanowires using X-ray diffraction[21−23] and X-ray fluorescence.[24]

Here, we present in operando electrical characterization of an InP nanowire field effect transistor exposed to hard X-rays (Figure 1). The measurements show that the X-ray induced conductance exceeds that expected from reported data by more than 5 orders of magnitude and that X-rays can be detected although the active volume is about 10^7 to 10^9 times smaller than the pixels of available semiconductor detectors. The effect is explained by time-resolved electrical measurements, which reveal characteristic lifetimes on the scale of seconds. To demonstrate the potential of nanowires as X-ray detectors, we use the nanowire to image the intensity distribution of a high flux synchrotron nanofocus.

The electrical response of InP nanowire field effect transistors[25,26] exposed to nanofocused hard X-rays (energy 13.8 keV, flux up to 2×10^9 ph/s) were investigated in ambient air (Figure 1a,b). Nanowires were synthesized and individually contacted as previously described.[25] In brief, the nanowires were doped with hydrogen sulfide (H_2S) during growth to have highly n-doped end segments (H_2S molar fraction $\chi = 7.1 \times 10^{-6}$, carrier concentration $n = 9 \times 10^{18}$ cm^{-3}), and a low-doped, highly resistive middle segment ($\chi = 3.3 \times 10^{-8}$, $n = 1 \times 10^{15}$ cm^{-3}). After growth, nanowires were transferred to a silicon wafer with a 100 nm thick insulating SiO_2 film and individually contacted using electron beam lithography. The distance between the two metal contacts was 3.2 μm. The highly doped end segments have high dark conductivity, and

Received: September 11, 2014
Revised: November 14, 2014

dx.doi.org/10.1021/nl5040545 | *Nano Lett.* XXXX, XXX, XXX−XXX

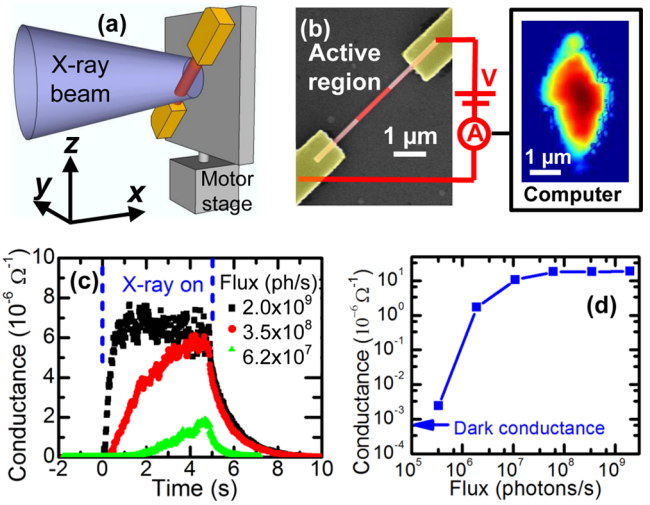

Figure 1. Hard X-ray detection in an InP nanowire transistor: (a) schematic of the experiment and (b) top-view scanning electron microscopy image of nanowire device, with bias voltage (V), the amperemeter (A), and the recording computer. The nanowire is false-colored pink, the high-resistivity active region in red, and metal contacts in yellow. (c) Conductance of the nanowire device as a function of time, for three different X-ray fluxes. The X-ray beam was turned on at t = 0 s and turned off at t = 4.9 s. (d) Maximum conductance vs X-ray flux.

the length of the active region was therefore the 1.4 μm low-doped middle segment.

We set a bias voltage, in the range 0.01 to 0.25 V, on one end of the nanowire, grounded the substrate and the other end, and measured the current with a picoammeter. The GINIX (Göttingen Instrument for Nano-Imaging with X-rays) end station at the P10 beamline at the PETRA III synchrotron, DESY, Hamburg, Germany, was used as X-ray source. The X-ray beam was perpendicular to the substrate. All the results in this letter come from the same device, but we have observed similar X-ray induced conductance in other devices.

When the device was exposed to X-rays, the electrical conductance increased from below 10^{-9} Ω^{-1} to about 10^{-5} Ω^{-1} (Figure 1c). X-ray induced conductance has previously been observed in large samples using a micron-sized beam.[7] The current–voltage dependence was linear both with and without X-ray excitation (Supporting Information Figure S1). The substrate gate was grounded in these experiments, but with a negative gate bias the dark conductance could be reduced to 10^{-12} Ω^{-1} for improved dynamic range.[25] We found that the conductance increased strongly with the X-ray flux Φ and was constant above $\Phi = 6.2 \times 10^7$ ph/s (Figure 1d).

Rough calculations show that the measured X-ray induced conductance significantly exceeds that expected from bulk parameters. The conductance is given by

$$G = \frac{q\mu}{l^2}N \qquad (1)$$

where N is the number of free electrons in the active region of the nanowire, l is the length of the active region, which was estimated from the nanowire segment growth times, and q the elementary charge, assuming that only electrons contribute with a mobility, μ, of 200 cm^2/(V s)[25] (Supporting Information section 2). The conductance of $G = 1.06 \times 10^{-5}$ Ω^{-1} at $\Phi = 1.1 \times 10^7$ ph/s corresponds to N = 6500 carriers. At the same time, the primary generation rate of electron–hole pairs is $\gamma = p_{abs}\eta\Phi$, where η = 3290 is the number of created electron–hole pairs per X-ray photon.[27] The absorption probability, p_{abs}, depends on the absorption length, 47 μm for InP at this photon energy, and the alignment of beam and nanowire and is estimated at $p_{abs} = 6.2 \times 10^{-4}$ (Supporting Information section 3). Thus, the carrier generation rate at this flux can be estimated at $\gamma \approx 2.2 \times 10^7$ s^{-1}. If the recombination lifetime would be similar to that reported from optical measurements on InP nanowires, $\tau_{BG} \approx 1$ ns,[8] the number of X-ray induced carriers at steady state would be $N = \gamma\tau_{BG} \approx 0.02$, over 5 orders of magnitude lower than needed for the observed conductance.

To investigate whether the dynamics in the nanowire was different from bulk, we turned the beam on and off while measuring the conductance (Figure 1c, 2, and S2, Supporting

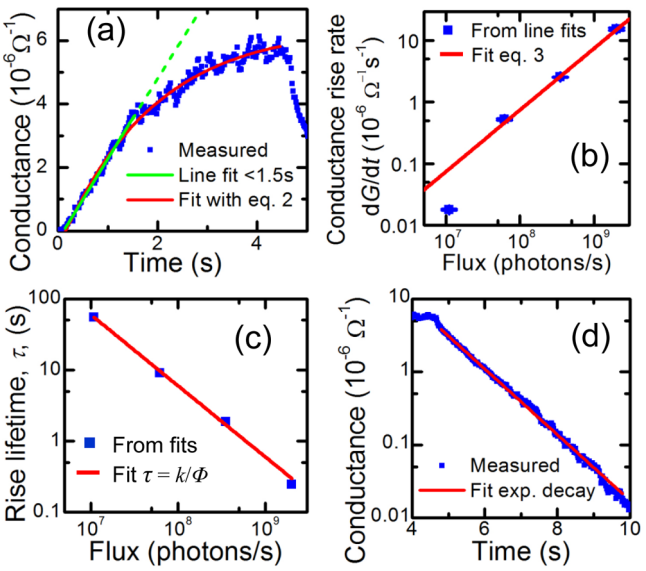

Figure 2. Dynamics of X-ray induced conductance. (a) Conductance vs time, $G(t)$, where the beam was turned on at t = 0 s and turned off at t = 4.6 s. X-ray flux 3.5×10^8 photons/s. Measured data in blue. Linear fit of the first 1.5 s in green, fit using eq 2 in red. (b) Conductance rise rate, dG/dt, evaluated from linear fits such as in panel a, vs flux, Φ, on a logarithmic scale. The red line shows a linear fit with slope 7.4×10^{-15} Ω^{-1}. (c) Conductance rise lifetime, τ, from fits using eq 2 such as in panel a, in blue, vs flux. The red line shows a fit of $\tau = k/\Phi$, with a slope $k = 6.0 \times 10^8$ Ω^{-1}. (d) Conductance vs time for decay part of the same measurement as in panel a, but on a semilogarithmic scale. The red curve shows an exponential decay fit with a lifetime τ = 0.97 s.

Information). The measurements revealed very long rise and decay times on a time scale of seconds. Photoconductivity experiments using UV light have revealed similarly slow processes in ZnO nanowires.[17] This was attributed to trapping of holes at the surface, leaving unbalanced conduction band electrons (photodoping). In addition, it is possible that trapped charges, which could reside on the surface or in the SiO_2 film, could gate the nanowire channel and increase the conductance by shifting the Fermi level (photogating).[28] The direct contribution to the nanowire conductance of photoelectrons induced in the substrate should be negligible since the SiO_2 film has a long X-ray absorption length and a small photoelectron escape depth (Supporting Information section 5).[29] Furthermore, substrate photoelectrons should prevent the high spatial resolution observed (see below). Preliminary experiments have also been done using nanowires oriented perpendicular to the

dx.doi.org/10.1021/nl5040545 | Nano Lett. XXXX, XXX, XXX–XXX

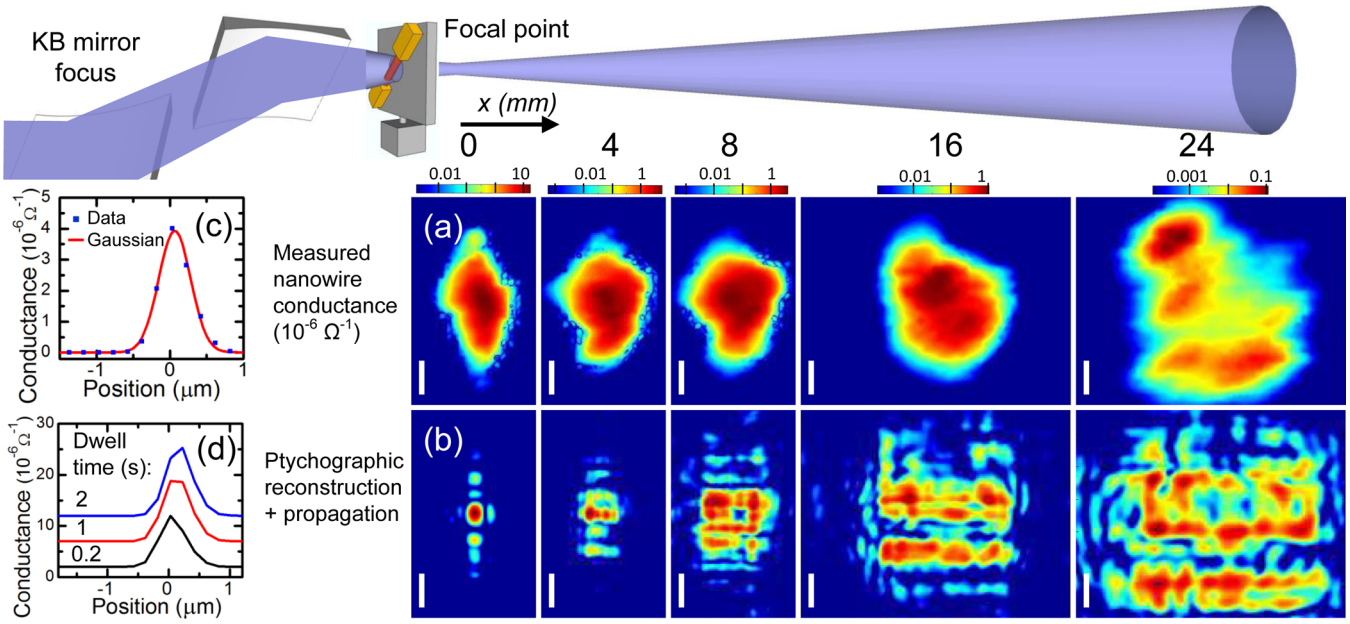

Figure 3. Direct imaging of an X-ray nanofocus: (a) imaging of a focused X-ray beam using the nanowire device, at different positions along the optical axis. Each image was normalized to its maximum conductance, and the logarithmic color scales show conductance (10^{-6} Ω^{-1}). (b) Reconstructed intensity of the same X-ray beam, using ptychography and Fresnel propagation. Each image was normalized to its maximum intensity. The color scale was chosen to have the same dynamic range as for the corresponding image in panel a: three orders of magnitude at x = 0, 4, and 8 mm, and 2 orders of magnitude at x = 16 and 24 mm. All scale bars are 1 μm. (c) Line scan of nanowire device through the focused X-ray beam. Data in blue, Gaussian fit with fwhm = 0.51 μm in red. (d) Line scans with different dwell times per point.

substrate with a wrap-around oxide (Supporting Information section 6).[30] In these devices the conducting channel is far from the substrate, but they still show a very strong X-ray induced conductance and long characteristic lifetimes. This demonstrates that the basic effect can be observed without influence of the substrate. In both geometries it is possible that traps in the oxide give a photodoping or photogating effect. Further experiments are needed to elucidate the underlying mechanism of the long characteristic lifetimes, and for simplicity, we only consider photodoping in the following.

The dynamic measurements can be used to estimate the characteristic lifetimes. The lack of large steps (Figure 1c) shows that the slow conductance increase cannot simply be accounted for by a small primary absorption since a single X-ray absorption event creates η = 3290 conduction band electron−hole pairs, corresponding to half of the maximum conductance. Most generated holes must recombine before being trapped, and to describe this effect we introduce a trapping probability p_{tr}. The rate equation for the number of electrons is then $dN/dt = p_{tr}\gamma - N/\tau$, where τ is the detrapping lifetime. For the rise after the beam is switched on, the boundary condition $N(0) = 0$ together with eq 1 leads to

$$G(t) = \frac{q\mu}{l^2} p_{tr}\gamma\tau(1 - \exp(-t/\tau)) \quad (2)$$

For small t, this can be linearized to $G(t) \approx q\mu/l^2 p_{tr}\gamma t$, with the time derivative (conductance rise rate)

$$\frac{dG}{dt} = \frac{q\mu}{l^2} p_{tr}\gamma = \frac{q\mu}{l^2} p_{tr}p_{abs}\eta\Phi \quad (3)$$

which is independent of τ and proportional to Φ.

Indeed, a linear increase in conductance is observed for early times (Figure 2a). We evaluated dG/dt vs Φ (Figure 2b) and found a linear relationship with a proportionality constant of 7.4×10^{-15} Ω^{-1}. Using eq 3, we can then estimate $p_{tr} \approx 2.3 \times 10^{-6}$. The low probability for hole trapping means that each X-ray absorption event generates at most one long-lived carrier, thereby explaining why no large steps are observed in the $G(t)$ plots. The nanosecond scale bandgap recombination was much too fast to capture with the present setup, but could be measurable with high-speed electronics.[17]

Next, the conductance increases were fitted using eq 2, using a single lifetime for each flux (Figures 2a,c and S2, Supporting Information). The lifetime exceeded 1 min for the lowest fluxes, while it was around 0.3 s for the full flux. We empirically found that the lifetime was inversely proportional to the flux for high fluxes ($\tau \approx 6.0 \times 10^8/\Phi$), meaning that the detrapping rate was proportional to the flux. Shutting the beam off showed exponential decays in conductance with lifetimes around 1 s (Figures 2d and S4, Supporting Information). The decay lifetimes were much shorter than the rise lifetimes at low flux, indicating different pathways for detrapping with and without X-ray flux.

The long characteristic lifetimes explain the strong X-ray induced conductance. For long times, the conductance saturates at $G(\infty) \approx (q\mu/l^2)p_{tr}p_{abs}\eta\Phi\tau$. Only a fraction, $p_{tr} \approx 2.3 \times 10^{-6}$, of the generated holes is trapped. However, since the lifetimes are about 10^9 to 10^{11} times τ_{BG}, the gain is still 10^3 to 10^5.

As a proof of concept of our nanowire device as a high-resolution detector, it was used to directly image the intensity distribution of a Kirkpatrick−Baez mirror nanofocus installed at the coherence beamline P10 of the PETRA III storage ring (Figure 3). Recording the current at a fixed bias of 0.1 V, 2D raster scans with a dwell time of 0.2 s per point were performed at several positions along the optical x-axis, resulting in a 3D characterization of the intensity profile (8 × 8 μm scan areas with 40 × 40 points). The results were compared a

dx.doi.org/10.1021/nl5040545 | Nano Lett. XXXX, XXX, XXX−XXX

ptychographic reconstruction of the beam (probe),[3,31−35] performed under identical parameters by scanning a different nanowire with partial overlap and inverting the far-field diffraction pattern.[36]

The resolution of the direct nanowire imaging was lower than the ptychographic reconstruction, but sufficient to show the overall diamond shape of the beam, and in good general agreement, see, for example, the three vertical substructures appear at similar distances as in the reconstruction (x = 24 mm defocus).

Since the spatial resolution was difficult to assess from 2D images, horizontal line scans across the beam (Figure 3c,d) were also performed. The measured fwhm in the line scans was about 0.51 μm. We varied the dwell time, device voltage, and flux (Supporting Information Figure S5) but found no systematic dependencies. The beam size (fwhm), as determined by ptychographic reconstruction, was 0.29 by 0.39 μm in the horizontal and vertical directions, respectively. Since our nanowire, oriented diagonally in the y-z plane, has a diameter of 100 nm, the effective size in the horizontal (y-axis) direction was 0.14 μm. Thus, the measured 0.51 μm is in reasonable agreement with a convolution of beam and detector sizes, and we conclude that the spatial resolution is limited by the nanowire size.

Two resolution limitations can be identified. First, the elongated shape of the diagonal nanowire blurs the 2D scans since the image is a convolution of the nanowire shape and the beam shape. Indeed, diagonal stripes are seen at x = 24 mm. By creating devices with the nanowire oriented orthogonal to the substrate,[37] parallel with the optical x-axis, the resolution would instead be limited by the smaller nanowire diameter. Second, the nanowire conductance was saturated since we used the full flux, and the nanowire conductance saturates around 6.2×10^7 ph/s (Figure 1d). This made it impossible to resolve the sharp central peak at focus and explains why smaller features can be observed in the lower-intensity, defocused beam at x = 24 mm. The high flux did not cause any measurable permanent damage to the device, however. Established X-ray detectors must typically be protected from the primary beam with beam stops in order to avoid damage.

In conclusion, we have demonstrated that the X-ray induced conductance in InP nanowire-FETs is up to 5 orders of magnitude larger than expected from a scaling of bulk parameters. Such effects may be present in any nanostructure exposed to X-rays since nanostructures by definition have high surface to volume ratios. More broadly, this shows that investigations with focused X-rays, despite the weak absorption, can strongly affect the sample under study. This work could be developed in the direction of sample characterization,[7] exploiting the long penetration depth, short pulses, and small foci of X-ray nanobeams.

Future developments in the direction of X-ray detection could explore shorter lifetimes for faster scan rates, for instance, by deposition of dielectrics.[38] Devices could be synthesized with the nanowire orientated along the beam, with lengths similar to X-ray absorption lengths.[39] In the Supporting Information, we present preliminary measurements of such devices. In this geometry the nanowire has much stronger primary absorption. The entire fields of view in the present experiment are smaller than single pixels of current direct-detection semiconductor devices.[5] Indirect detectors based on scintillators and optical microscopes can reach spatial resolutions of slightly below 1 μm, but future improvements are difficult since this is near the diffraction limit.[40] In contrast, the spatial resolution in nanowire-based sensors would be limited by the nanowire diameter, which can be as low as a few nanometers.[41,42] Semiconductor nanowires may therefore enable a novel kind of high-resolution scanning X-ray detectors, especially suitable for near-field X-ray detection in small-focus and high-flux applications. Such detectors could complement, and even be used simultaneously with, traditional far field detectors.

METHODS

The same sensitivity of the picoammeter was used for all measurements. The currents were in the range 10 pA to 2 μA.

For the imaging shown in Figure 3, we used 8 × 8 μm scan areas with 40 × 40 points. The measured piezo motor positions were used for the analysis.

For the measurements in Figure 1d, the beam was left on for several minutes in order to measure $G(\infty)$. The dynamic measurements for the high fluxes (Figure 1c all fluxes; Figure 2a,b all fluxes; Figure 2c two highest fluxes) were made a few hours later with a higher sampling rate and shorter time, and the analysis after the beamtime revealed 50−70% lower $G(\infty)$ for these measurements. We tentatively attribute this to drift in the sample stage. This discrepancy prevents a meaningful comparison of the measured $G(\infty)$ in Figure 1d, with the $G(\infty)$ that can be calculated using the relation $G(\infty) \approx (q\mu/l^2)$ $p_{tr}p_{abs}\eta\Phi\tau$ and the lifetimes in Figure 2c. For the rise lifetimes in Figure 2c, we used the later measurements with high sampling rate for the two highest fluxes, and the earlier measurements with long measurement times for the two lower fluxes.

Ptychography is a powerful technique for analyzing coherent X-ray wavefields.[3,31−34] The ptychographic reconstruction of the illuminating wave field (probe) was carried out by scanning a test structure (semiconductor nanowires on a Si_3N_4 membrane) on a rectangular grid perpendicular to the optical axis and close to the focal plane, as separately reported in detail.[36] Diffraction patterns of the scattered intensity were recorded by using the Lambda detector,[36,43] which was placed at 5.07 m downstream of the sample. A chosen region of 160 × 160 pixels around the beam of each diffraction pattern defines the pixel size in the probe and object plane to be about 52 nm (small angle approximation). The ePIE algorithm was used for obtaining the reconstruction.[35] The algorithm was run for 600 iterations where the probe reconstruction was averaged over the last 200 iterations.

ASSOCIATED CONTENT

Supporting Information

Current−voltage measurements, derivation of eq 1, absorption probability, further dynamic measurements, contribution of substrate photoelectrons, vertical nanowire device, and resolution optimization. This material is available free of charge via the Internet at http://pubs.acs.org.

AUTHOR INFORMATION

Corresponding Author

*E-mail: jwallen@uni-goettingen.de.

Author Contributions

J.W., M.O., R.W., M.S., and T.S. performed the measurements. J.W., K.M.P., and L.E.W. made the samples. The manuscript

dx.doi.org/10.1021/nl5040545 | Nano Lett. XXXX, XXX, XXX−XXX

was written through contributions of all authors. All authors have given approval to the final version of the manuscript.

Notes

The authors declare no competing financial interest.

■ ACKNOWLEDGMENTS

We thank Magnus Borgström for nanowire samples, Karl Lautscham and Claes Thelander for help with the sample holder, and Martin Krenkel for assistance with measurements. Financial support by the K. A. Wallenberg Foundation and SFB 755 'Nanoscale Photonic Imaging' of the Deutsche Forschungsgemeinschaft is gratefully acknowledged

■ REFERENCES

(1) Döring, F.; Robisch, A. L.; Eberl, C.; Osterhoff, M.; Ruhlandt, A.; Liese, T.; Schlenkrich, F.; Hoffmann, S.; Bartels, M.; Salditt, T.; Krebs, H. U. Sub-5 nm hard x-ray point focusing by a combined Kirkpatrick-Baez mirror and multilayer zone plate. *Opt. Express* **2013**, *21* (16), 19311−19323.

(2) Mimura, H.; Handa, S.; Kimura, T.; Yumoto, H.; Yamakawa, D.; Yokoyama, H.; Matsuyama, S.; Inagaki, K.; Yamamura, K.; Sano, Y.; Tamasaku, K.; Nishino, Y.; Yabashi, M.; Ishikawa, T.; Yamauchi, K. Breaking the 10 nm barrier in hard-X-ray focusing. *Nat. Phys.* **2010**, *6* (2), 122−125.

(3) Schropp, A.; Boye, P.; Feldkamp, J. M.; Hoppe, R.; Patommel, J.; Samberg, D.; Stephan, S.; Giewekemeyer, K.; Wilke, R. N.; Salditt, T.; Gulden, J.; Mancuso, A. P.; Vartanyants, I. A.; Weckert, E.; Schoder, S.; Burghammer, M.; Schroer, C. G. Hard X-ray nanobeam characterization by coherent diffraction microscopy. *Appl. Phys. Lett.* **2010**, *96* (9), 091102−3.

(4) Chao, W.; Harteneck, B. D.; Liddle, J. A.; Anderson, E. H.; Attwood, D. T. Soft X-ray microscopy at a spatial resolution better than 15 nm. *Nature* **2005**, *435* (7046), 1210−1213.

(5) Denes, P.; Schmitt, B. Pixel detectors for diffraction-limited storage rings. *J. Synchrotron Radiat.* **2014**, *21* (5), 1006−1010.

(6) Ziaja, B.; London, R. A.; Hajdu, J. Ionization by impact electrons in solids: Electron mean free path fitted over a wide energy range. *J. Appl. Phys.* **2006**, *99* (3), 033514.

(7) Vyvenko, O. F.; Buonassisi, T.; Istratov, A. A.; Hieslmair, H.; Thompson, A. C.; Schindler, R.; Weber, E. R. X-ray beam induced current-a synchrotron radiation based technique for the in situ analysis of recombination properties and chemical nature of metal clusters in silicon. *J. Appl. Phys.* **2002**, *91* (6), 3614−3617.

(8) Joyce, H. J.; Wong-Leung, J.; Yong, C.-K.; Docherty, C. J.; Paiman, S.; Gao, Q.; Tan, H. H.; Jagadish, C.; Lloyd-Hughes, J.; Herz, L. M.; Johnston, M. B. Ultralow surface recombination velocity in InP nanowires probed by terahertz spectroscopy. *Nano Lett.* **2012**, *12* (10), 5325−5330.

(9) Durbin, S. M.; Clevenger, T.; Graber, T.; Henning, R. X-ray pump optical probe cross-correlation study of GaAs. *Nat. Photonics* **2012**, *6* (2), 111−114.

(10) Nirmal, M.; Dabbousi, B. O.; Bawendi, M. G.; Macklin, J. J.; Trautman, J. K.; Harris, T. D.; Brus, L. E. Fluorescence intermittency in single cadmium selenide nanocrystals. *Nature* **1996**, *383* (6603), 802−804.

(11) Chan, C. K.; Peng, H.; Liu, G.; McIlwrath, K.; Zhang, X. F.; Huggins, R. A.; Cui, Y. High-performance lithium battery anodes using silicon nanowires. *Nat. Nanotechnol.* **2008**, *3* (1), 31−35.

(12) Wernersson, L. E.; Thelander, C.; Lind, E.; Samuelson, L. III-V Nanowires-extending a narrowing road. *Proc. IEEE* **2010**, *98* (12), 2047−2060.

(13) Wallentin, J.; Anttu, N.; Asoli, D.; Huffman, M.; Åberg, I.; Magnusson, M. H.; Siefer, G.; Fuss-Kailuweit, P.; Dimroth, F.; Witzigmann, B.; Xu, H. Q.; Samuelson, L.; Deppert, K.; Borgström, M. T. InP nanowire array solar cells achieving 13.8% efficiency by exceeding the ray optics limit. *Science* **2013**, *339* (6123), 1057−1060.

(14) Nam, S.-W.; Chung, H.-S.; Lo, Y. C.; Qi, L.; Li, J.; Lu, Y.; Johnson, A. T. C.; Jung, Y.; Nukala, P.; Agarwal, R. Electrical wind force-driven and dislocation-templated amorphization in phase-change nanowires. *Science* **2012**, *336* (6088), 1561−1566.

(15) Mourik, V.; Zuo, K.; Frolov, S. M.; Plissard, S. R.; Bakkers, E. P. A. M.; Kouwenhoven, L. P. Signatures of Majorana fermions in hybrid superconductor-semiconductor nanowire devices. *Science* **2012**, *336* (6084), 1003−1007.

(16) Wang, J. F.; Gudiksen, M. S.; Duan, X. F.; Cui, Y.; Lieber, C. M. Highly polarized photoluminescence and photodetection from single indium phosphide nanowires. *Science* **2001**, *293* (5534), 1455−1457.

(17) Soci, C.; Zhang, A.; Xiang, B.; Dayeh, S. A.; Aplin, D. P. R.; Park, J.; Bao, X. Y.; Lo, Y. H.; Wang, D. ZnO nanowire UV photodetectors with high internal gain. *Nano Lett.* **2007**, *7* (4), 1003−1009.

(18) Pettersson, H.; Trägårdh, J.; Persson, A. I.; Landin, L.; Hessman, D.; Samuelson, L. Infrared photodetectors in heterostructure nanowires. *Nano Lett.* **2006**, *6* (2), 229−232.

(19) Misra, S.; Liu, N.; Nelson, J.; Hong, S. S.; Cui, Y.; Toney, M. F. In situ X-ray diffraction studies of (de)lithiation mechanism in silicon nanowire anodes. *ACS Nano* **2012**, *6* (6), 5465−5473.

(20) Weinhausen, B.; Saldanha, O.; Wilke, R. N.; Dammann, C.; Priebe, M.; Burghammer, M.; Sprung, M.; Köster, S. Scanning X-ray nanodiffraction on living eukaryotic cells in microfluidic environments. *Phys. Rev. Lett.* **2014**, *112* (8), 088102.

(21) Favre-Nicolin, V.; Mastropietro, F.; Eymery, J.; Camacho, D.; Niquet, Y. M.; Borg, B. M.; Messing, M. E.; Wernersson, L. E.; Algra, R. E.; Bakkers, E. P. A. M.; Metzger, T. H.; Harder, R.; Robinson, I. K. Analysis of strain and stacking faults in single nanowires using Bragg coherent diffraction imaging. *New J. Phys.* **2010**, *12* (3), 035013.

(22) Newton, M. C.; Leake, S. J.; Harder, R.; Robinson, I. K. Three-dimensional imaging of strain in a single ZnO nanorod. *Nat. Mater.* **2010**, *9* (2), 120−124.

(23) Diaz, A.; Mocuta, C.; Stangl, J.; Mandl, B.; David, C.; Vila-Comamala, J.; Chamard, V.; Metzger, T. H.; Bauer, G. Coherent diffraction imaging of a single epitaxial InAs nanowire using a focused x-ray beam. *Phys. Rev. B* **2009**, *79* (12), 125324.

(24) Segura-Ruiz, J.; Martínez-Criado, G.; Chu, M. H.; Geburt, S.; Ronning, C. Nano-X-ray Absorption Spectroscopy of Single Co-Implanted ZnO Nanowires. *Nano Lett.* **2011**, *11* (12), 5322−5326.

(25) Wallentin, J.; Ek, M.; Wallenberg, L. R.; Samuelson, L.; Borgström, M. T. Electron Trapping in InP Nanowire FETs with Stacking Faults. *Nano Lett.* **2011**, *12* (1), 151−155.

(26) Cui, Y.; Duan, X. F.; Hu, J. T.; Lieber, C. M. Doping and electrical transport in silicon nanowires. *J. Phys. Chem. B* **2000**, *104* (22), 5213−5216.

(27) Suzuki, Y.; Fukuda, Y.; Nagashima, Y.; Kan, H. An indium phosphide solid state detector: A possible low energy gamma and neutrino detector. *Nucl. Instrum. Methods Phys. Res., Sect. A* **1989**, *275* (1), 142−148.

(28) Thunich, S.; Prechtel, L.; Spirkoska, D.; Abstreiter, G.; Morral, A. F. I.; Holleitner, A. W. Photocurrent and photoconductance properties of a GaAs nanowire. *Appl. Phys. Lett.* **2009**, *95* (8), 083111.

(29) Seah, M. P. Simple universal curve for the energy-dependent electron attenuation length for all materials. *Surf. Interface Anal.* **2012**, *44* (10), 1353−1359.

(30) Persson, K. M.; Berg, M.; Borg, M. B.; Jun, W.; Johansson, S.; Svensson, J.; Jansson, K.; Lind, E.; Wernersson, L. E. Extrinsic and intrinsic performance of vertical InAs nanowire MOSFETs on Si substrates. *IEEE Trans. Electron Devices* **2013**, *60* (9), 2761−2767.

(31) Rodenburg, J. M.; Hurst, A. C.; Cullis, A. G.; Dobson, B. R.; Pfeiffer, F.; Bunk, O.; David, C.; Jefimovs, K.; Johnson, I. Hard-X-ray lensless imaging of extended objects. *Phys. Rev. Lett.* **2007**, *98* (3), 034801.

(32) Thibault, P.; Dierolf, M.; Menzel, A.; Bunk, O.; David, C.; Pfeiffer, F. High-resolution scanning X-ray diffraction microscopy. *Science* **2008**, *321* (5887), 379−382.

(33) Takahashi, Y.; Suzuki, A.; Furutaku, S.; Yamauchi, K.; Kohmura, Y.; Ishikawa, T. High-resolution and high-sensitivity phase-contrast

imaging by focused hard x-ray ptychography with a spatial filter. *Appl. Phys. Lett.* **2013**, *102* (9), 094102−4.
(34) Godard, P.; Carbone, G.; Allain, M.; Mastropietro, F.; Chen, G.; Capello, L.; Diaz, A.; Metzger, T. H.; Stangl, J.; Chamard, V. Three-dimensional high-resolution quantitative microscopy of extended crystals. *Nat. Commun.* **2011**, *2*, 568.
(35) Maiden, A. M.; Rodenburg, J. M. An improved ptychographical phase retrieval algorithm for diffractive imaging. *Ultramicroscopy* **2009**, *109* (10), 1256−1262.
(36) Wilke, R. N.; Wallentin, J.; Osterhoff, M.; Pennicard, D.; Zozulya, A.; Sprung, M.; Salditt, T. High-flux ptychographic imaging using the new 55 mm pixel detector Lambda based on the Medipix3 readout chip. *Acta Crystallogr., Sect. A* **2014**, *A70* (6), 552−562.
(37) Ng, H. T.; Han, J.; Yamada, T.; Nguyen, P.; Chen, Y. P.; Meyyappan, M. Single crystal nanowire vertical surround-gate field-effect transistor. *Nano Lett.* **2004**, *4* (7), 1247−1252.
(38) Munch, S.; Reitzenstein, S.; Borgström, M.; Thelander, C.; Samuelson, L.; Worschech, L.; Forchel, A. Time-resolved photoluminescence investigations on HfO_2-capped InP nanowires. *Nanotechnology* **2010**, *21* (10), 105711.
(39) Ramdani, M. R.; Gil, E.; Leroux, C.; AndreÌ, Y.; Trassoudaine, A.; Castelluci, D.; Bideux, L.; Monier, G.; Robert-Goumet, C.; Kupka, R. Fast growth synthesis of GaAs nanowires with exceptional length. *Nano Lett.* **2010**, *10* (5), 1836−1841.
(40) Martin, T.; Koch, A. Recent developments in X-ray imaging with micrometer spatial resolution. *J. Synchrotron Radiat.* **2006**, *13* (2), 180−194.
(41) Gil, E.; Dubrovskii, V. G.; Avit, G.; André, Y.; Leroux, C.; Lekhal, K.; Grecenkov, J.; Trassoudaine, A.; Castelluci, D.; Monier, G.; Ramdani, R. M.; Robert-Goumet, C.; Bideux, L.; Harmand, J. C.; Glas, F. Record pure zincblende phase in GaAs nanowires down to 5 nm in radius. *Nano Lett.* **2014**, *14* (7), 3938−3944.
(42) Zhang, J. J.; Katsaros, G.; Montalenti, F.; Scopece, D.; Rezaev, R. O.; Mickel, C.; Rellinghaus, B.; Miglio, L.; De Franceschi, S.; Rastelli, A.; Schmidt, O. G. Monolithic growth of ultrathin Ge nanowires on Si(001). *Phys. Rev. Lett.* **2012**, *109* (8), 085502.
(43) Pennicard, D.; Lange, S.; Smoljanin, S.; Hirsemann, H.; Graafsma, H.; Epple, M.; Zuvic, M.; Lampert, M. O.; Fritzsch, T.; Rothermund, M. The LAMBDA photon-counting pixel detector. *J. Phys.: Conf. Ser.* **2013**, *425* (6), 062010.